

911 **Chapter 4**  
912 **Classical Cyclotron**

913 **Abstract** This chapter introduces to the classical cyclotron, and to the theoretical  
914 material needed for the simulation exercises. It begins with a brief reminder of the  
915 historical context, and continues with beam optics and acceleration techniques which  
916 the classical cyclotron principle and methods lean on, including  
917 - ion orbit in a cyclic accelerator,  
918 - weak focusing and periodic transverse motion,  
919 - revolution period and isochronism,  
920 - voltage gap and resonant acceleration,  
921 - the cyclotron equation.

922  
923 Simulation of a cyclotron dipole will either resort to an analytical model of the  
924 field: the optical element DIPOLE, or will otherwise resort to a field map and to  
925 the keyword TOSCA to handle it and raytrace through, An additional accelerator  
926 device needed in the exercises, CAVITE, simulates a local oscillating voltage. Run-  
927 ning a simulation generates a variety of output files, including the execution listing  
928 zgoubi.res, always, and other zgoubi.plt, zgoubi.CAVITE.out, zgoubi.MATRIX.out,  
929 etc., aimed at looking up program execution, storing data for post-treatment, pro-  
930 ducing graphs, etc. Additional keywords are introduced as needed, such as FIT[2],  
931 a matching procedure; FAISCEAU and FAISTORE which log local particle data in  
932 zgoubi.res or in a user defined ancillary file; MARKER; the 'system call' command  
933 SYSTEM; REBELOTE, a 'do loop'; and some more. This chapter introduces in addi-  
934 tion to spin motion in accelerator magnets; dedicated simulation exercises include a  
935 variety of keywords: SPNTRK, a request for spin tracking, SPNPRT or FAISTORE,  
936 to log spin vector components in respectively zgoubi.res or some ancillary file, and  
937 the "IL=2" flag to log stepwise particle data, including spin vector, in zgoubi.plt file.  
938 Simulations include deriving transport matrices, beam matrix, optical functions and  
939 their transport, from rays, using MATRIX and TWISS keywords.

940 **Notations used in the Text**

$B; B_0$	field value; at reference radius $R_0$
$\mathbf{B}; B_R; B_y$	field vector; radial component; axial component
$B\rho = p/q$	ion rigidity
$C; C_0$	orbit length, $C = 2\pi R$ ; reference, $C_0 = 2\pi R_0$
$E$	ion energy
$f_{\text{rev}}, f_{\text{rf}}$	revolution and accelerating voltage frequencies
$h$	harmonic number, an integer, $h = f_{\text{rf}}/f_{\text{rev}}$
$k = \frac{R}{B} \frac{dB}{dR}$	radial field index
$m; m_0; M$	mass, $m = \gamma m_0$ ; rest mass; in units of $\text{MeV}/c^2$
$\mathbf{p}; p; p_0$	ion momentum vector; its modulus; reference
$q$	ion charge
$R; R_0; R_E$	orbit radius; reference radius $R(p_0)$ ; at energy $E$
$RF$	Radio-Frequency: as per the accelerating voltage technology
941 $s$	path variable
$T_{\text{rev}}, T_{\text{rf}}$	revolution and accelerating voltage periods
$\mathbf{v}; v$	ion velocity vector; its modulus
$V(t); \hat{V}$	oscillating voltage; its peak value
$x, x', y, y'$	radial and axial coordinates in the moving frame [ $(*)' = d(*)/ds$ ]
$\alpha$	momentum compaction, or trajectory deviation
$\beta = v/c; \beta_0; \beta_s$	normalized ion velocity; reference; synchronous
$\gamma = E/m_0$	Lorentz relativistic factor
$\Delta p, \delta p$	momentum offset
$\epsilon_u$	Courant-Snyder invariant (u: x, r, y, l, Y, Z, s, etc.)
$\theta$	azimuthal angle
$\phi$	RF phase at ion arrival at the voltage gap

942 **4.1 Introduction**

943 Cyclotrons are the most widespread type of accelerator, today, used by hundreds,  
 944 with dominant application the production of isotopes. This chapter is devoted to the  
 945 first cyclic accelerator: the 1930s “classical” cyclotron which its concept limited to  
 946 low energy, a few 10s of  $\text{MeV}/\text{nucleon}$ , a limitation overcome a decade later by the  
 947 azimuthally varying field (AVF) technique - subject of the next chapter.

948 The 1930s cyclotron is based on two main principles:

949 (i) resonant acceleration by synchronization of a fixed-frequency accelerating voltage  
 950 on the quasi-constant revolution time, an acceleration technique still in use a century  
 951 later, and

952 (ii) transverse beam confinement based on so-called weak focusing, a technique  
 953 which would be used over the years in all (but the AVF) cyclic accelerators: cyclotron,  
 954 microtron, betatron, synchrotron, until the invention of alternating gradient strong

955 focusing in the early 1950s; weak focusing it is still in use today, in betatrons and  
 956 low energy proton synchrotrons mostly.

957 The cyclotron concept goes back to the late 1920s [1], a cyclotron was first brought  
 958 to operation in the early 1930s [2], its principles are summarized in Fig. 4.1: an  
 959 oscillating voltage is applied on a pair of electrodes (“dees”) forming an accelerating  
 960 gap and placed between the two poles of an electromagnet; ions reaching the gap  
 961 during the acceleration phase of the voltage wave experience an energy boost; under  
 962 the effect of energy increase, they spiral out in the quasi-constant field of the dipole.  
 The first cyclotron achieved acceleration of  $H_2^+$  hydrogen ions to 80 keV [2], at

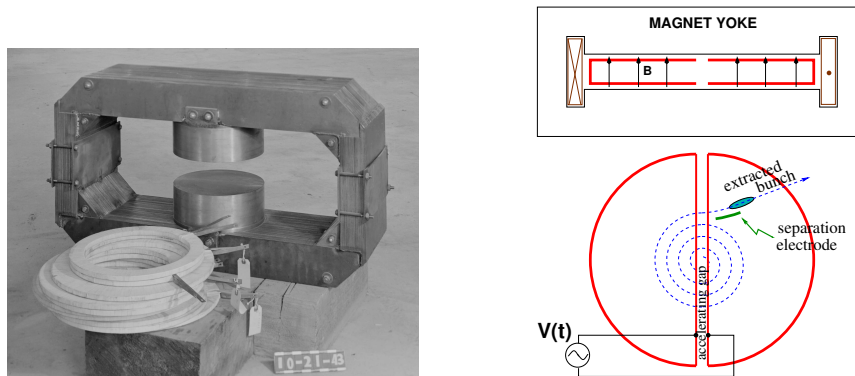


**Fig. 4.1** Left: dipole electromagnet used for a model of Berkeley’s 184-inch cyclotron, in 1943 [3]. Right: a schematic view of the resonant acceleration method: in the uniform field between the two cylindrical magnetic poles (top), accelerated ions spiral out (bottom); a double-dee (or, a variant, a single-dee facing a slotted electrode) forms a gap to which is applied a fixed-frequency oscillating voltage  $V(t)$  of which the frequency is a harmonic of the revolution frequency; ions experiencing proper voltage phase at the gap are accelerated; a septum electrode allows beam extraction

963 Berkeley in 1931. The apparatus used a dee-shaped electrode vis-à-vis a slotted  
 964 electrode forming a voltage gap, the ensemble housed in a 5 inch diameter vacuum  
 965 chamber and placed in the 1.3 Tesla field of an electromagnet. A  $\approx 12$  MHz vacuum  
 966 tube oscillator provided a 1 kVolt gap voltage.  
 967

968 One goal foreseen in developing this technology was the acceleration of protons  
 969 to MeV energy range for the study of atom nucleus - and in background a wealth of  
 970 potential applications. An 11 inch cyclotron followed which delivered a  $0.01 \mu A H_2^+$   
 971 beam at 1.22 MeV [4], and a 27 inch cyclotron later reached 6 MeV (Fig. 4.2) [5].  
 972 Targets were mounted at the periphery of the 11 inch cyclotron, disintegrations were  
 973 observed in 1932. And, in 1933: *‘The neutron had been identified by Chadwick*  
 974 *in 1932. By 1933 we were producing and observing neutrons from every target*  
 975 *bombarded by deuterons.*“ [5, M.S. Livingston, p. 22].

976 A broad range of applications were foreseen: *‘At this time biological experiments*  
 977 *were started. [...] Also at about this same time the first radioactive tracer experiments*  
 978 *on human beings were tried [...] simple beginnings of therapeutic use, coming a*

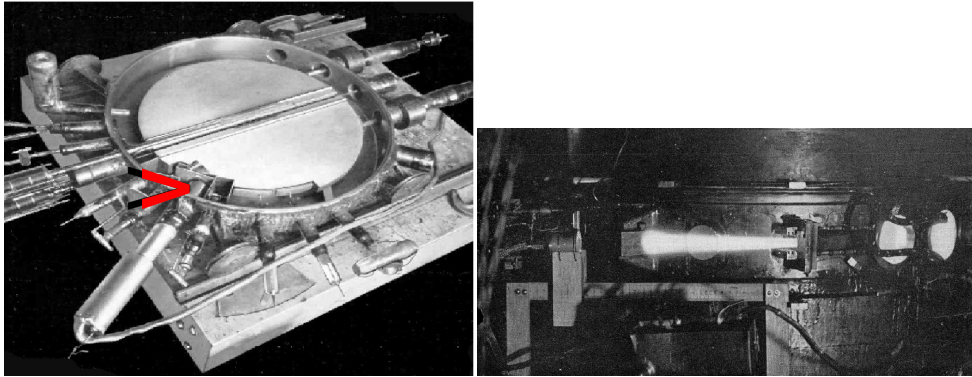


**Fig. 4.2** Berkeley 27 inch cyclotron, brought to operation in 1934, accelerated deuterons up to 6 MeV. Left: a double-dee (seen in the vacuum chamber, cover off), 22 inch diameter, creates an accelerating gap: 13 kV, 12 MHz radio frequency voltage is applied for deuterons for instance (through two feed lines seen at the right). This apparatus was dipped in the 1.6 Tesla dipole field of a 27 in diameter, 75 ton, electromagnet. A slight decrease of the dipole field with radius, from the center of the dipole, assures axial beam focusing. With their energy increasing, ions spiral out from the center to eventually strike a target (arrow). Right: ionization of the air by the extracted beam (1936); the view also shows the vacuum chamber squeezed between the pole pieces of the electromagnet [3]

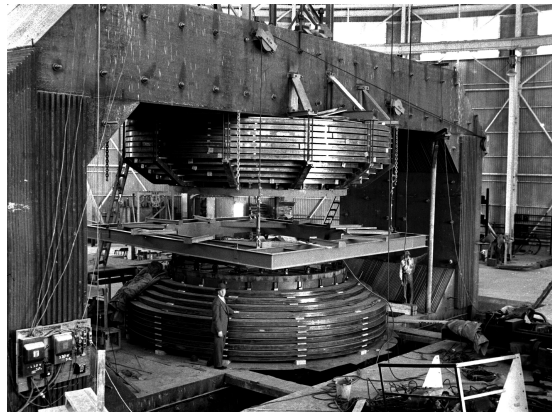


**Fig. 4.3** Berkeley 184 in diameter, 4,000 ton cyclotron during construction [3]. Its design was modified and it was operated as a synchrocyclotron from the beginning, in 1946

979 *little bit later, in which neutron radiation was used, for instance, in the treatment*  
 980 *of cancer. [...] Another highlight from 1936 was the first time that anyone tried*  
 981 *to make artificially a naturally occurring radio-nuclide. (a bismuth isotope) [5,*  
 982 *McMillan, p. 26].*

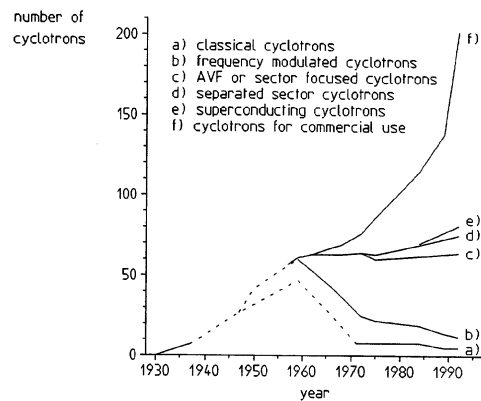
983 *Limitation in energy*

984 A complete understanding of ion dynamics in the classical cyclotron took more or  
 985 less until the mid-1930s and brought two news, a bad one and a good one,

986 (i) bad one first: the energy limitation, a consequence of the loss of isochronism  
 987 resulting from the relativistic increase of the ion mass so that “[...] *it seems useless*  
 988 *to build cyclotrons of larger proportions than the existing ones [...] an accelerating*  
 989 *chamber of 37 in radius will suffice to produce deuterons of 11 MeV energy which*  
 990 *is the highest possible [...]*” [6], or in a different form: “*If you went to graduate*  
 991 *school in the 1940s, this inequality ( $-1 < k < 0$ ) was the end of the discussion of*  
 992 *accelerator theory*” [7].

993 (ii) the good news now: the overcoming of the energy limit which results from the  
 994 mass increase, by splitting the magnetic pole into valley and hill field sectors: the  
 995 azimuthally varying field (AVF) cyclotron, by L.H. Thomas in 1938 [8] - the object  
 996 of Chapt. 5. It took some years to see effects of this breakthrough.

**Fig. 4.4** Evolution of the number of the various cyclotron species, over the years [9] [10, Fig. 8]. From the 1950s on the AVF cyclotron rapidly supplanted the 1930s' classical cyclotron



997 With the progress in magnet computation tools, in computational speed and  
 998 beam dynamics simulations, the AVF cyclotron ends up being essentially as simple  
 999 to design and build has in a general manner supplanted the classical cyclotron in all  
 1000 energy domains (Fig. 4.4).

1001 **4.2 Basic Concepts and Formulae**

1002 The cyclotron was conceived as a means to overcome the technological difficulty of  
 1003 a long series of high electrostatic voltage electrodes in a linear layout, by, instead,  
 1004 repeated recirculation through a single accelerating gap in synchronism with an  
 1005 oscillating voltage (Fig. 4.5). With its energy increasing, an accelerated bunch spirals  
 1006 out in the uniform magnetic field, the velocity increase comes with an increase in orbit

**Fig. 4.5** Resonant acceleration: in an  $h = 1$  configuration an ion bunch meets an oscillating field  $\vec{E}$  across gap A, at time  $t$ , on accelerating phase; it meets again, half a turn later, at time  $t + T_{\text{rev}}/2$ , the accelerating phase across gap A', and so on: the uniform magnetic field recirculates the bunch through the gap, repeatedly. Higher harmonic allows more bunches: the next possibility with two dees is  $h=3$ , and 3 bunches, 120 degrees apart, in synchronism with  $\vec{E}$

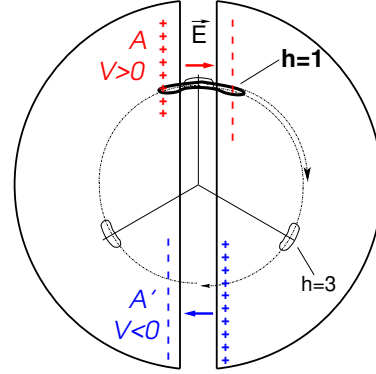
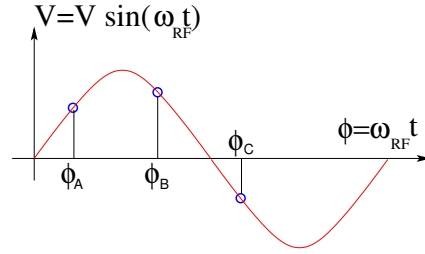


**Fig. 4.6** A ion which reaches the double-dee gap at the RF phase  $\omega_{\text{rf}}t = \phi_A$  or  $\omega_{\text{rf}}t = \phi_B$  is accelerated. If it reaches the gap at  $\omega_{\text{rf}}t = \phi_C$  it is decelerated



1007 length; the net result is a slow increase of the revolution period  $T_{\text{rev}}$  with energy, yet,  
 1008 with appropriate fixed voltage frequency  $f_{\text{rf}} \approx h/T_{\text{rev}}$  the revolution motion and the  
 1009 oscillating voltage can be maintained in sufficiently close synchronism,  $T_{\text{rev}} \approx hT_{\text{rf}}$ ,  
 1010 that the bunch will transit the voltage gap upon accelerating phase (Fig. 4.6) over a  
 1011 large enough number of turns that it acquires a significant energy boost.

1012 The orbital motion quantities: radius  $R$ , ion rigidity  $BR$ , revolution frequency  
 1013  $f_{\text{rev}}$ , satisfy

$$BR = \frac{p}{q}, \quad 2\pi f_{\text{rev}} = \omega_{\text{rev}} = \frac{v}{R} = \frac{qB}{m} = \frac{qB}{\gamma m_0} \quad (4.1)$$

1014 relationships which hold at all  $\gamma$ , so covering the *classical* cyclotron domain ( $v \ll c$ ,  
 1015  $\gamma \approx 1$ ) as well as the *isochronous* cyclotron (ion energy increase commensurate with  
 1016 its mass - Chapt. 5). To give an idea of the revolution frequency, in the limit  $\gamma = 1$ ,  
 1017 for protons, one has  $f_{\text{rev}}/B = q/2\pi m = 15.25 \text{ MHz/T}$ .

1018 The cyclotron design sets the constant RF frequency  $f_{\text{rf}} = \omega_{\text{rf}}/2\pi$  at an interme-  
 1019 diate value of  $hf_{\text{rev}}$  along the acceleration cycle. The energy gain, or loss, by the ion  
 1020 when transiting the gap, at time  $t$ , is

$$\Delta W(t) = q\hat{V} \sin \phi(t) \quad \text{with} \quad \phi(t) = \omega_{\text{rf}}t - \omega_{\text{rev}}t + \phi_0 \quad (4.2)$$

with  $\phi$  its phase with respect to the RF signal at the gap (Fig. 4.6),  $\phi_0 = \phi(t = 0)$ ,  
 and  $\omega_{\text{rev}}t$  the orbital angle. Assuming constant field  $B$ , the increase of the revolution

period with ion energy satisfies

$$\frac{\Delta T_{\text{rev}}}{T_{\text{rev}}} = \gamma - 1$$

1021 The mis-match so induced between the RF and cyclotron frequencies is a turn-by-turn  
1022 cumulative effect and sets a limit to the tolerable isochronism defect,  $\Delta T_{\text{rev}}/T_{\text{rev}} \approx$   
1023  $2 - 3\%$ , or highest velocity  $\beta = v/c \approx 0.22$ . This results for instance in a practical  
1024 limitation to  $\approx 25$  MeV for protons, and  $\approx 50$  MeV for D and  $\alpha$  particles.

1025 Over time multiple-gap accelerating structures were developed, whereby a  
1026 “multiple- $\Delta$ ” electrode pattern substitutes a “double-D”. An example is GANIL  
1027 C0 injector with its 4 accelerating gaps and  $h = 4$  and  $h = 8$  RF harmonic operation  
1028 [11].

#### 1029 4.2.1 Fixed-Energy Orbits, Revolution Period

In a laboratory frame (O;x,y,z), with (O;x,z) the bend plane (Fig. 4.7), assume  $\mathbf{B}|_{y=0} = \mathbf{B}_y$ , constant. An ion is launched from the origin with a velocity

$$\mathbf{v} = \left( \frac{dx}{dt}, \frac{dy}{dt}, \frac{dz}{dt} \right) = (v \sin \alpha, 0, v \cos \alpha)$$

1030 at an angle  $\alpha$  from the z-axis.

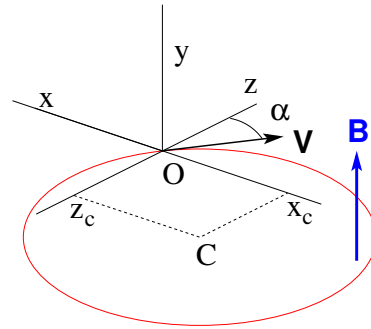


**Fig. 4.7** Circular motion of an ion in the plane normal to a uniform magnetic field  $\mathbf{B}$ . The orbit is centered at  $x_C = -v \cos \alpha / \omega_{\text{rev}}$ ,  $z_C = v \sin \alpha / \omega_{\text{rev}}$ , its radius is  $v / \omega_{\text{rev}}$

1031 Solving

$$m\dot{\mathbf{v}} = q\mathbf{v} \times \mathbf{B} \quad (4.3)$$

1032 with  $\mathbf{B} = (0, B_y, 0)$  yields the parametric equations of motion

$$\begin{cases} x(t) = \frac{v}{\omega_{\text{rev}}} \cos(\omega_{\text{rev}}t - \alpha) - \frac{v \cos \alpha}{\omega_{\text{rev}}} \\ y(t) = \text{constant} z(t) = \frac{v}{\omega_{\text{rev}}} \sin(\omega_{\text{rev}}t - \alpha) + \frac{v \sin \alpha}{\omega_{\text{rev}}} \end{cases} \quad (4.4)$$

1033 which result in

$$\left(x + \frac{v \cos \alpha}{\omega_{\text{rev}}}\right)^2 + \left(z - \frac{v \sin \alpha}{\omega_{\text{rev}}}\right)^2 = \left(\frac{v}{\omega_{\text{rev}}}\right)^2 \quad (4.5)$$

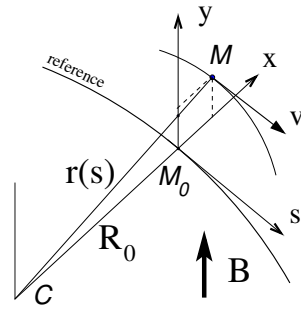
1034 a circular trajectory of radius  $R = v/\omega_{\text{rev}}$  centered at  $(x_C, z_C) = \left(-\frac{v \cos \alpha}{\omega_{\text{rev}}}, \frac{v \sin \alpha}{\omega_{\text{rev}}}\right)$ .

1035 *Stability of the cyclic motion* - The initial velocity vector defines a, say “reference”,  
 1036 closed orbit in the median plane of the cyclotron dipole; a small perturbation in  $\alpha$  or  
 1037  $v$  defines a new orbit *in the vicinity* of the reference. An axial velocity component  $v_y$   
 1038 on the other hand, causes the ion to drift away from the reference, vertically, linearly  
 1039 with time, as there is no axial restoring force. The next Section will investigate the  
 1040 necessary field property to ensure both horizontal and vertical confinement of the  
 1041 cyclic motion in the vicinity of a reference orbit in the median plane.

#### 1042 4.2.2 Weak Focusing, Linearized Approach

1043 In the early accelerated turns in a classical cyclotron (central region of the electro-  
 1044 magnet, energy up to tens of keV/u), the accelerating electric field provides adequate  
 1045 transverse focusing [11], whereas a flat magnetic field with uniformity  $dB/B < 10^{-4}$   
 1046 is sufficient to maintain isochronism. Beyond this low energy region however, at  
 1047 greater radii, a magnetic field gradient must be introduced to ensure transverse  
 1048 stability: field must decrease with  $R$ .

**Fig. 4.8** Moving frame  
 ( $M_0; s, x, y, s$ ) along the ref-  
 erence circular orbit. The cur-  
 vature  $1/R_0$  is constant along  
 the orbit and ( $M_0; s, x, y$ )  
 can be considered equiva-  
 lent to the cylindrical frame  
 ( $C; \theta, R_0, y$ )



1049 Ion coordinates in the following are defined in the moving frame ( $M_0; s, x, y$ )  
 1050 (Fig. 4.8), which moves along the reference orbit (radius  $R_0$ ), with its origin  $M_0$   
 1051 the projection of ion location  $M$  on the reference orbit; the  $s$  axis is tangent to the



1052 latter, the  $x$  axis is normal to  $s$ , the  $y$  axis is normal to the bend plane. Median-plane  
 1053 symmetry of the field is assumed, thus the radial field component  $B_R|_{y=0} = 0$  at all  
 1054  $R$  (Fig. 4.9).

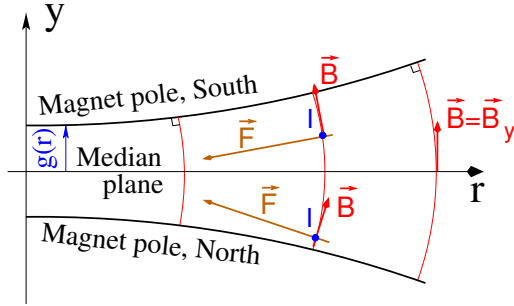
1055 Consider small motion excursions from  $(R = R_0, y = 0)$ :  $x(t) = R(t) - R_0 \ll R_0$ ;  
 1056 introduce the Taylor expansion of the vertical field component

$$\begin{aligned}
 B_y(R_0 + x) &= B_y(R_0) + x \left. \frac{\partial B_y}{\partial R} \right|_{R_0} + \frac{x^2}{2!} \left. \frac{\partial^2 B_y}{\partial R^2} \right|_{R_0} + \dots \approx B_y(R_0) + x \left. \frac{\partial B_y}{\partial R} \right|_{R_0} \\
 B_R(0 + y) &= y \left. \frac{\partial B_R}{\partial y} \right|_0 + \frac{y^3}{3!} \left. \frac{\partial^3 B_R}{\partial y^3} \right|_0 + \dots \approx y \left. \frac{\partial B_y}{\partial R} \right|_{R_0} \\
 &= \left. \frac{\partial B_y}{\partial R} \right|_{R_0} y
 \end{aligned} \quad (4.6)$$

1057 Using these, and noting  $(\dot{*}) = d(*)/dt$ , the linear approximation of the differential  
 1058 equations of motion in the moving frame writes

$$\begin{aligned}
 F_x = m\ddot{x} &= -qvB_y(R) + \frac{mv^2}{R_0 + x} \approx -qv \left( B_y(R_0) + \left. \frac{\partial B_y}{\partial R} \right|_{R_0} x \right) + \frac{mv^2}{R_0} \left( 1 - \frac{x}{R_0} \right) \\
 \rightarrow m\ddot{x} &= -\frac{mv^2}{R_0^2} \left( \frac{R_0}{B_0} \left. \frac{\partial B_y}{\partial R} \right|_{R_0} + 1 \right) x \\
 F_y = m\ddot{y} &= qvB_R(y) = qv \left. \frac{\partial B_R}{\partial y} \right|_{y=0} y + \text{higher order} \rightarrow m\ddot{y} = qv \left. \frac{\partial B_y}{\partial R} \right|_{R_0} y
 \end{aligned} \quad (4.7)$$

**Fig. 4.9** Axial motion stability requires proper shaping of field lines:  $B_y$  has to decrease with radius. The Laplace force pulls a positive charge with velocity pointing out of the page, at I, toward the median plane. Increasing the field gradient ( $k$  closer to -1, gap opening up faster) increases the focusing



1059 Note  $B_y(R_0) = B_0$  and introduce  
 1060

$$\omega_R^2 = \omega_{\text{rev}}^2 \left( 1 + \frac{R_0}{B_0} \left. \frac{\partial B_y}{\partial R} \right|_{R_0} \right), \quad \omega_y^2 = -\omega_{\text{rev}}^2 \frac{R_0}{B_0} \left. \frac{\partial B_y}{\partial R} \right|_{R_0} \quad (4.8)$$

1061 substitute in Eqs. 4.7, this yields

**Fig. 4.10** Geometrical focusing: in a uniform field,  $k=0$ , the two circular trajectories at  $r = R_0 \pm \delta R$  (solid lines) undergo exactly one oscillation around the reference orbit  $r = R_0$ . A positive  $k$  (square markers) increases the convergence - but causes the vertical motion to diverge; a negative  $k$  (triangles), a necessary condition for axial focusing, decreases the convergence

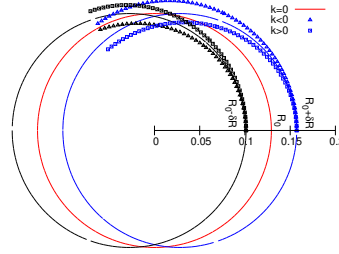
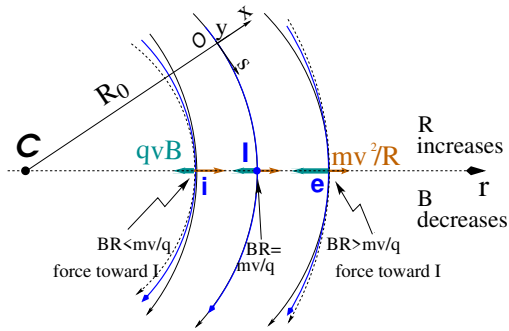


**Fig. 4.11** Radial motion stability in an axially symmetric structure. Trajectories arcs at  $p=mv$  are represented: case of  $k=0$  (thin black lines), of  $-1 < k < 0$  (thick blue lines), and of  $k=-1$  (dashed concentric circles).  $k$  decreasing towards  $-1$  reduces the geometrical focusing, increases axial focusing. The resultant of the Laplace and centrifugal forces,  $F_t = -qvB + mv^2/r$ , is zero at  $I$ , motion is stable if  $F_t$  is toward  $I$  at  $i$ , i.e.  $qvB_i < mv^2/R_i$ , and toward  $I$  as well at  $e$ , i.e.  $qvB_e > mv^2/R_e$



$$\ddot{x} + \omega_R^2 x = 0 \quad \text{and} \quad \ddot{y} + \omega_y^2 y = 0 \quad (4.9)$$

1062 A restoring force (linear terms in  $x$  and  $y$ , Eq. 4.9) arises from the radially varying  
1063 field, characterized by a field index

$$k = \frac{R_0}{B_0} \left. \frac{\partial B_y}{\partial R} \right|_{R=R_0, y=0} \quad (4.10)$$

1064 *Radial stability* - radially this force adds to the geometrical focusing (curvature  
1065 term “1” in  $\omega_R^2$ , Eq. 4.8, Fig. 4.10). In the weakly decreasing field  $B(R)$  an ion  
1066 with momentum  $p = mv$  moving in the vicinity of the  $R_0$ -radius reference orbit  
1067 experiences in the moving frame a resultant force  $F_t = -qvB + m \frac{v^2}{r}$  (Fig. 4.11) of  
1068 which the (outward) component  $f_c = m \frac{v^2}{r}$  decreases with  $r$  at a higher rate than the  
1069 decrease of the Laplace (inward) component  $f_B = -qvB(r)$ . In other words, radial

1070 stability requires  $BR$  to increase with  $R$ ,  $\frac{\partial BR}{\partial R} = B + R\frac{\partial B}{\partial R} > 0$ , this holds in particular  
1071 at  $R_0$ , thus  $1 + k > 0$ .

1072 *Axial stability* requires a restoring force directed toward the median plane. Refer-  
1073 ring to Fig. 4.9, this means  $F_y = -a \times y$  (with  $a$  a positive quantity) and thus  $B_R < 0$ ,  
1074 at all  $(r, y \neq 0)$ . This is achieved by designing a guiding field which decreases with  
1075 radius,  $\frac{\partial B_R}{\partial y} < 0$ . Referring to Eq. 4.10 this means  $k < 0$ .

1076 From these radial and axial constraints the condition of “weak focusing” for  
1077 transverse motion stability around the circular equilibrium orbit results, namely,

$$-1 < k < 0 \quad (4.11)$$

Note regarding the geometrical focusing: the focal distance associated with the curvature of a magnet of arc length  $\mathcal{L}$  is obtained by integrating  $\frac{d^2x}{ds^2} + \frac{1}{R_0^2}x = 0$  and identifying with the focusing property  $\Delta x' = -x/f$ , namely,

$$\Delta x' = \int \frac{d^2x}{ds^2} ds \approx \frac{-x}{R^2} \int ds = \frac{-x\mathcal{L}}{R^2}, \text{ thus } f = \frac{R^2}{\mathcal{L}}$$

1078 *Isochronism*: the axial focusing constraint:  $B$  decreasing with  $R$ , contributes break-  
1079 ing the isochronism (in addition to the effect of the mass increase) by virtue of  
1080  $\omega_{\text{rev}} \propto B$ .

#### 1081 *Paraxial Transverse Coordinates*

1082 Introduce the path variable,  $s$ , as the independent variable in Eq. 4.9 and neglect the  
1083 transverse velocity components:  $ds \approx v dt$ ; the equations of motion in the moving  
1084 frame (Eq. 4.9) thus take the form

$$\frac{d^2x}{ds^2} + \frac{1+k}{R_0^2}x = 0 \quad \text{and} \quad \frac{d^2y}{ds^2} - \frac{k}{R_0^2}y = 0 \quad (4.12)$$

1085 Given  $-1 < k < 0$  the motion is that of a harmonic oscillator, in both planes, with  
1086 respective restoring constants  $(1+k)/R_0^2$  and  $-k/R_0^2$ , both positive quantities. The  
1087 solution is a sinusoidal motion,

$$\begin{cases} R(s) - R_0 = x(s) = x_0 \cos \frac{\sqrt{1+k}}{R_0}(s - s_0) + x'_0 \frac{R_0}{\sqrt{1+k}} \sin \frac{\sqrt{1+k}}{R_0}(s - s_0) \\ R'(s) = x'(s) = -x_0 \frac{\sqrt{1+k}}{R_0} \sin \frac{\sqrt{1+k}}{R_0}(s - s_0) + x'_0 \cos \frac{\sqrt{1+k}}{R_0}(s - s_0) \end{cases} \quad (4.13)$$

$$\begin{cases} y(s) = y_0 \cos \frac{\sqrt{-k}}{R_0}(s - s_0) + y'_0 \frac{R_0}{\sqrt{-k}} \sin \frac{\sqrt{-k}}{R_0}(s - s_0) \\ y'(s) = -y_0 \frac{\sqrt{-k}}{R_0} \sin \frac{\sqrt{-k}}{R_0}(s - s_0) + y'_0 \cos \frac{\sqrt{-k}}{R_0}(s - s_0) \end{cases} \quad (4.14)$$

1089 Radial and axial wave numbers can be introduced,

$$v_R = \frac{\omega_R}{\omega_{\text{rev}}} = \sqrt{1+k} \quad \text{and} \quad v_y = \frac{\omega_y}{\omega_{\text{rev}}} = \sqrt{-k} \quad (4.15)$$

1090 *i.e.*, the number of sinusoidal oscillations of the paraxial motion about the reference  
 1091 circular orbit over a turn, respectively radial and axial. Both are less than 1: there  
 1092 is less than one sinusoidal oscillation in a revolution. In addition, as a result of the  
 1093 axial symmetry,

$$v_R^2 + v_y^2 = 1 \quad (4.16)$$

#### 1094 *Off-Momentum Motion*

In an axially symmetric structure, the equilibrium trajectory at momentum  $\begin{cases} p_0 \\ p = p_0 + \Delta p \end{cases}$

is at radius  $\begin{cases} R_0 \text{ such that } B_0 R_0 = p_0/q \\ R \text{ such that } BR = p/q \end{cases}$ , with  $\begin{cases} B = B_0 + \left(\frac{\partial B}{\partial x}\right)_0 \Delta x + \dots \\ R = R_0 + \Delta x \end{cases}$

On the other hand

$$BR = \frac{p}{q} \Rightarrow \left[ B_0 + \left(\frac{\partial B}{\partial x}\right)_0 \Delta x + \dots \right] (R_0 + \Delta x) = \frac{p_0 + \Delta p}{q}$$

1095 which, neglecting terms in  $(\Delta x)^2$ , and given  $B_0 R_0 = \frac{p_0}{q}$ , leaves  $\Delta x \left[ \left(\frac{\partial B}{\partial x}\right)_0 R_0 + B_0 \right] = \frac{\Delta p}{q}$ . With  $k = \frac{R_0}{B_0} \left(\frac{\partial B}{\partial x}\right)_0$  this yields

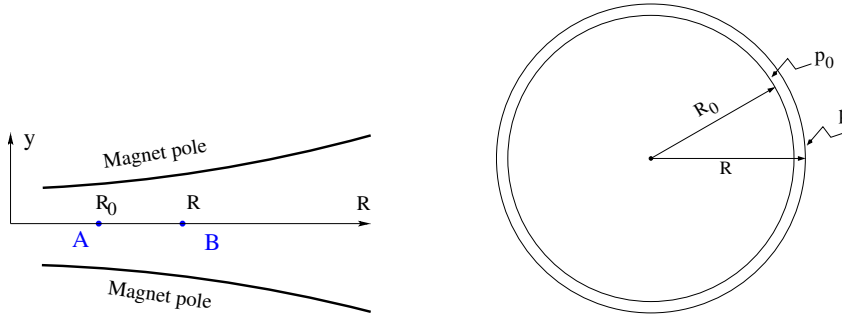


**Fig. 4.12** The equilibrium radius at location A is  $R_0$ , the equilibrium momentum is  $p_0$ , rigidity is  $B_0 R_0$ . The equilibrium radius at B is  $R$ , equilibrium momentum  $p$ , rigidity  $BR$

1096

$$\Delta x = D \frac{\Delta p}{p_0} \quad \text{with} \quad D = \frac{R_0}{1+k} \quad \text{the dispersion function} \quad (4.17)$$

1097 The dispersion  $D$  is an  $s$ -independent quantity as a result of the cylindrical symmetry  
 1098 of the field ( $k$  and  $R=p/qB$  are  $s$ -independent).

1099 To the first order in the coordinates, the vertical coordinates  $y(s)$ ,  $y'(s)$  (Eq. 4.14)  
 1100 are unchanged under the effect of a momentum offset, the horizontal trajectory angle  
 1101  $x'(s)$  (Eq. 4.13) is unchanged as well (the circular orbits are concentric, Fig. 4.12)  
 1102 whereas  $x(s)$  satisfies

$$x(s, p_0 + \Delta p) = x(s, p_0) + \Delta p \left. \frac{\partial x}{\partial p} \right|_{s, p_0} = x(s, p_0) + D \frac{\Delta p}{p_0} \quad (4.18)$$

1103 *Orbit and revolution period lengthening*

1104 A  $p + \delta p$  off-momentum motion satisfies (Eq. 4.17)

$$\frac{\delta C}{C} = \frac{\delta R}{R} = \frac{\delta x}{R} = \alpha \frac{\delta p}{p} \quad \text{with} \quad \alpha = \frac{1}{1+k} = \frac{1}{v_R^2} \quad (4.19)$$

1105 with  $\alpha$  the ‘‘momentum compaction’’, a positive quantity: orbit length increases with  
 1106 momentum. Substituting  $\frac{\delta \beta}{\beta} = \frac{1}{\gamma^2} \frac{\delta p}{p}$ , the change in revolution period  $T_{\text{rev}} = C/\beta c$   
 1107 with momentum writes

$$\frac{\delta T_{\text{rev}}}{T_{\text{rev}}} = \frac{\delta C}{C} - \frac{\delta \beta}{\beta} = \left( \alpha - \frac{1}{\gamma^2} \right) \frac{\delta p}{p} \quad (4.20)$$

1108 Given that  $-1 < k < 0$  and  $\gamma \gtrsim 1$ , it results that  $\alpha - 1/\gamma^2 > 0$ : the revolution period  
 1109 increases with energy, the increase in radius is faster than the velocity increase.

### 1110 4.2.3 Quasi-Isochronous Resonant Acceleration

1111 The energy  $W$  of an accelerated ion (in the non-relativistic energy domain, which is  
 1112 that of the classical cyclotron) satisfies the frequency dependence

$$W = \frac{1}{2} m v^2 = \frac{1}{2} m (2\pi R f_{\text{rev}})^2 = \frac{1}{2} m \left( 2\pi R \frac{f_{\text{rf}}}{h} \right)^2 \quad (4.21)$$

1113 Observe in passing: given the cyclotron size (radius  $R$ ),  $f_{\text{rf}}$  and  $h$  set the limit for  
 1114 the acceleration range. The revolution frequency decreases with energy and the  
 1115 condition of synchronism with the oscillating voltage,  $f_{\text{rf}} = h f_{\text{rev}}$ , is only fulfilled  
 1116 at that particular radius where  $\omega_{\text{rf}} = qB/m$  (Fig. 4.13-left). The out-phasing  $\Delta\phi$  of  
 1117 the RF at ion arrival at the gap builds-up turn after turn, decreasing in a first stage  
 1118 (towards lower voltages in Fig. 4.13-right) and then increasing back to  $\phi = \pi/2$  and  
 1119 beyond towards  $\pi$ . Beyond  $\phi = \pi$  the RF voltage is decelerating.

1120 With  $\omega_{\text{rev}}$  constant between two gap passages, differentiating  $\phi(t)$  (Eq. 4.2) yields  
 1121  $\dot{\phi} = \omega_{\text{rf}} - \omega_{\text{rev}}$ . Between two gap passages on the other hand,  $\Delta\phi = \dot{\phi} \Delta T = \dot{\phi} T_{\text{rev}}/2 =$   
 1122  $\dot{\phi} \frac{\pi R}{v}$ , yielding a phase-shift of

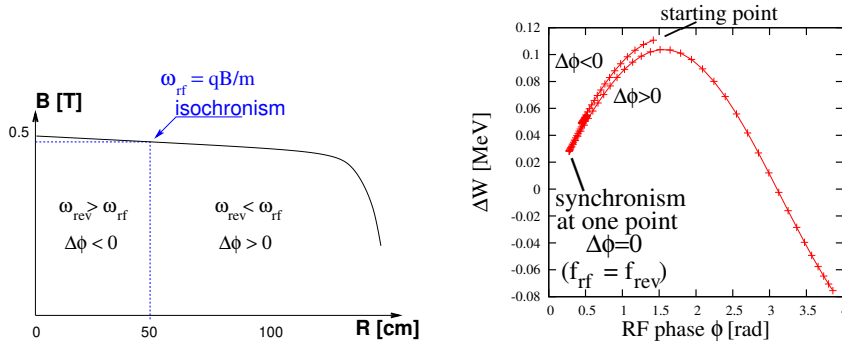
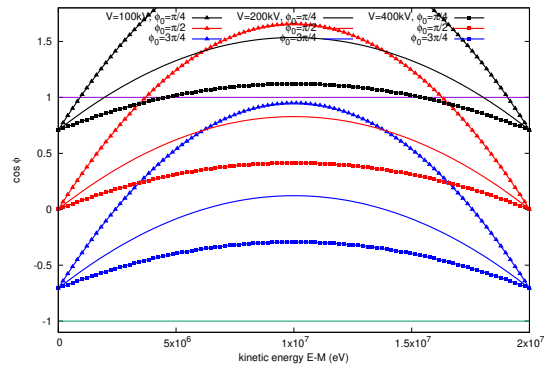


**Fig. 4.13** A sketch of the synchronism condition at one point (left,  $h=1$  assumed), and the span in phase of the energy gain  $\Delta W = q\hat{V} \sin \phi$  (Eq. 4.2) over the acceleration cycle (right). The two  $\Delta W(\phi)$  branches on the right graph ( $\Delta\phi < 0$  and  $\Delta\phi > 0$ ) actually superimpose, they have been dissociated here for clarity

$$\text{half-turn } \Delta\phi = \pi \left( \frac{\omega_{\text{rf}}}{\omega_{\text{rev}}(R)} - 1 \right) = \pi \left( \frac{m\omega_{\text{rf}}}{qB(R)} - 1 \right) \quad (4.22)$$

1123 The out-phasing is thus a gap-after-gap, cumulative effect. Due to this the classical  
 1124 cyclotron requires quick acceleration (limited number of turns), which means high  
 1125 voltage (tens to hundreds of kVolts). As expected, with  $\omega_{\text{rf}}$  and  $B$  constant,  $\phi$  presents  
 1126 a minimum ( $\dot{\phi} = 0$ ) at  $\omega_{\text{rf}} = \omega_{\text{rev}} = qB/m$  where exact isochronism is reached  
 1127 (Fig. 4.13). The upper limit to  $\phi$  is set by the condition  $\Delta W > 0$ : acceleration.

**Fig. 4.14** A graph of the cyclotron equation (Eq. 4.23), for a few different settings of the accelerating voltage. The sole settings resulting in  $-1 < \cos \phi(E) < 1, \forall E$ , allow complete acceleration to top energy.  $\phi_i = \pi/4$  at injection for instance, does not allow acceleration to 20 MeV (upper three curves). Acceleration to 20 MeV works with  $\phi_i = 3\pi/4$ , with as low as 100 kV/gap (lower three curves)



1128 The cyclotron equation determines the achievable energy range, depending on  
 1129 the injection energy  $E_i$ , the RF phase at injection  $\phi_i$ , the RF frequency  $\omega_{\text{rf}}$  and gap  
 1130 voltage  $\hat{V}$ , and writes [12]

$$\cos \phi = \cos \phi_i + \pi \left[ 1 - \frac{\omega_{rf}}{\omega_{rev}} \frac{E + E_i}{2M} \right] \frac{E - E_i}{q\hat{V}} \quad (4.23)$$

1131 and is represented in Fig. 4.14 for various values of the peak voltage and phase at  
 1132 injection  $\phi_i$ .  $M$  and  $E$  are respectively the rest mass and relativistic energy in  $\text{eV}/c^2$   
 1133 units,  $q\hat{V}$  is expressed in electron-volts, the index  $i$  denotes injection parameters.

#### 1134 4.2.4 Beam Extraction

1135 From  $R = p/qB$  and assuming  $B(R) \approx \text{constant}$  (this is legitimate as  $k$  is normally  
 1136 small), in the non-relativistic approximation ( $W \ll M$ ,  $W = p^2/2M$ ) one gets

$$\frac{dR}{R} = \frac{1}{2} \frac{dW}{W} \quad (4.24)$$

1137 Integrating yields

$$R^2 = R_i^2 \frac{W}{W_i} \quad (4.25)$$

1138 with  $R_i$ ,  $W_i$  initial conditions. From Eqs. 4.24, 4.25, assuming  $W_i \ll W$  and constant  
 1139 acceleration rate  $dW$  such that  $W = n dW$  after  $n$  turns, one gets the scaling laws

$$R \propto \sqrt{n}, \quad dR \propto \frac{R}{W} \propto \frac{1}{R} \propto dW, \quad \frac{dR}{dn} = \frac{R}{2n} \quad (4.26)$$

1140 Thus, in particular, the turn separation  $dR/dn$  is proportional to the orbit radius  $R$   
 1141 and to the energy gain per turn.

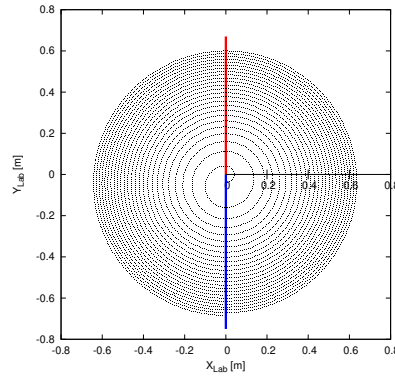


**Fig. 4.15** The radial distance between successive turns decreases with energy, in inverse proportion to the orbit radius

1142 The radial distance between successive turns decreases with energy, toward zero  
 1143 (Fig. 4.15), eventually resulting in insufficient spacing for insertion of an extraction  
 1144 septum.

1145 *Orbit modulation*

1146 Consider an ion bunch injected in the cyclotron with some  $(x_0, x'_0)$  conditions in the  
 1147 vicinity of the reference orbit, and assume very slow acceleration. While accelerated  
 1148 the bunch undergoes an oscillatory motion around the local closed orbit (Eq. 4.13).  
 1149 Observed at the extraction septum this oscillation modulates the distance of the  
 1150 bunch to the local reference closed orbit, moving it outward or inward depending on  
 1151 the turn number, which modulates the distance between the accelerated turns. This  
 1152 effect can be exploited to increase the separation between the final two turns and so  
 1153 enhance the extraction efficiency [9].

1154 **4.2.5 Spin Dance**

1155 The magnetic field  $\mathbf{B}$  of the cyclotron dipole exerts a torque on the spin angular  
 1156 momentum  $\mathbf{S}$  of an ion, causing it to precess following the Thomas-BMT differential  
 1157 equation [13]

$$\frac{d\mathbf{S}}{dt} = \mathbf{S} \times \underbrace{\frac{q}{m} [(1+G)\mathbf{B}_{\parallel} + (1+G\gamma)\mathbf{B}_{\perp}]}_{\omega_{\text{sp}}} \quad (4.27)$$

1158 wherein  $t$  is the time;  $\omega_{\text{sp}}$  the precession vector: a combination of  $\mathbf{B}_{\parallel}$  and  $\mathbf{B}_{\perp}$   
 1159 components of  $\mathbf{B}$  respectively parallel and orthogonal to the ion velocity vector.  $G$   
 1160 is the gyromagnetic anomaly,

1161  $G=1.7928474$  (proton),  $-0.178$  (Li),  $-0.143$  (deuteron),  $-4.184$  ( $^3\text{He}$ ) ...

1162  $\mathbf{S}$  in this equation is in the ion rest frame, all other quantities are in the laboratory  
 1163 frame.

1164 In the case of an ion moving in the median plane of the dipole,  $\mathbf{B}_{\parallel} = 0$ , thus the  
 1165 precession axis is parallel to the magnetic field vector,  $\mathbf{B}_y$ , so that  $\omega_{\text{sp}} = \frac{q}{m} (1 +$   
 1166  $G\gamma)\mathbf{B}_y$ . The precession angle over a trajectory arc  $\mathcal{L}$  is

$$\theta_{\text{sp, Lab}} = \frac{1}{v} \int_{(\mathcal{L})} \omega_{\text{sp}} ds = (1+G\gamma) \frac{\int_{(\mathcal{L})} B ds}{BR} = (1+G\gamma)\alpha \quad (4.28)$$

1167 with  $\alpha$  the trajectory deviation angle (Fig. 4.16). The precession angle in the moving  
 1168 frame (the latter rotates by an angle  $\alpha$  along  $\mathcal{L}$ ) is

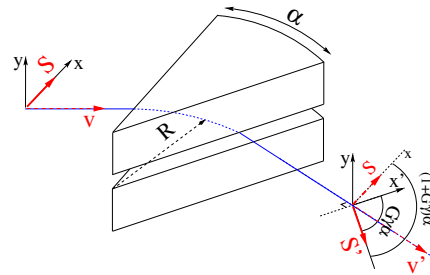
$$\theta_{\text{sp}} = G\gamma\alpha \quad (4.29)$$

1169 thus the number of  $2\pi$  spin precessions per ion orbit around the cyclotron is  $G\gamma$ . By  
 1170 analogy with the wave numbers (Eq. 4.15) this defines the “spin tune”

$$\nu_{\text{sp}} = G\gamma \quad (4.30)$$



**Fig. 4.16** Spin and velocity vector precession in a constant field, from  $\mathbf{S}$  to  $\mathbf{S}'$  and  $\mathbf{v}$  to  $\mathbf{v}'$  respectively. In the moving frame the spin precession along the arc  $\mathcal{L} = R\alpha$  is  $G\gamma\alpha$ , in the laboratory frame the spin precesses by  $(1 + G\gamma)\alpha$



### 1171 4.3 Exercises

#### 1172 4.1 Modeling a Cyclotron Dipole: Using a Field Map

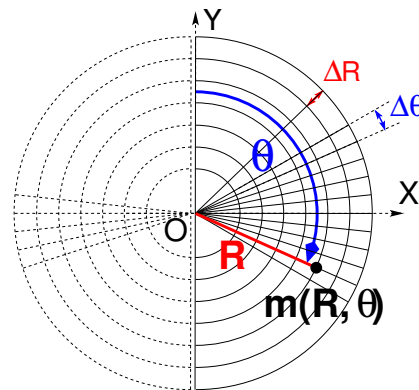
1173 Solution: page 259

1174 In this exercise, ion trajectories are ray-traced, various optical properties addressed  
1175 in the foregoing are recovered, using a field map to simulate the cyclotron dipole.  
1176 Fabricating that field map is a preliminary step of the exercise.

1177 The interest of using a field map is that it is an easy way to account for fancy magnet  
1178 geometries and fields, including field gradients and possible defects. A field map can  
1179 be generated using mathematical field models, or from magnet computation codes, or  
1180 from magnetic measurements. The first method is used, here. TOSCA keyword [14,  
1181 *cf.* INDEX] is used to ray-trace through the map.

1182 *Working hypotheses:* A 2-dimensional  $m(R, \theta)$  polar meshing of the median plane  
1183 is considered (Fig. 4.17). It is defined in a  $(O; X, Y)$  frame and covers an angular  
1184 sector of a few tens of degrees. The mid-plane field map is the set of values  $B_Z(R, \theta)$   
1185 at the nodes of the mesh. During ray-tracing, TOSCA extrapolates the field along  
1186 3D space  $(R, \theta, Z)$  ion trajectories from the 2D map [14].

**Fig. 4.17** Principle of a 2D field map in polar coordinates, covering a  $180^\circ$  sector (over the right hand side dee). The mesh nodes  $m(R, \theta)$  are distant  $\Delta R$  radially,  $\Delta\theta$  azimuthally. The map is used twice to cover the  $360^\circ$  cyclotron dipole as sketched here, while allowing insertion of an accelerating gap between the two dees



1187 (a) Construct a  $180^\circ$  two-dimensional map of a median plane field  $B_Z(R, \theta)$ ,  
1188 proper to simulate the field in a cyclotron as sketched in Fig. 4.1. Use one of the  
1189 following two methods: either (i) write an independent program, or (ii) use `zgoubi`  
1190 and its analytical field model `DIPOLE`, together with the keyword `CONSTY` [14,  
1191 *cf.* INDEX].

1192 Besides: use a uniform mesh (Fig. 4.17) covering from  $R_{\min}=1$  to  $R_{\max}=76$  cm,  
1193 with radial increment  $\Delta R = 0.5$  cm, azimuthal increment  $\Delta\theta = 0.5$  [cm]/ $R_0$  with  $R_0$   
1194 some reference radius (say, 50 cm, in view of subsequent exercises), and constant  
1195 axial field  $B_Z = 0.5$  T. The appropriate 6-column formatting of the field map data  
1196 for TOSCA to read is the following:

1197  $R \cos \theta, Z, R \sin \theta, B_Y, B_Z, B_X$

1198 with  $\theta$  varying first,  $R$  varying second;  $Z$  is the vertical direction (normal to the map  
1199 mesh),  $Z \equiv 0$  in the present case. Note that proper functioning of TOSCA requires  
1200 the field map to begin with the following line of numerical values:

1201  $R_{\min}$  [cm]  $\Delta R$  [cm]  $\Delta\theta$  [deg]  $Z$  [cm]

1202 Produce a graph of the  $B_Z(R, \theta)$  field map content.

1203 (b) Ray-trace a few concentric circular mid-plane trajectories centered on the  
1204 center of the dipole, ranging in  $10 \leq R \leq 80$  cm. Produce a graph of these concentric  
1205 trajectories in the  $(O; X, Y)$  laboratory frame.

1206 Initial coordinates can be defined using OBJET, particle coordinates along tra-  
1207 jectories during the stepwise ray-tracing can be logged in zgoubi.plt by setting IL=2  
1208 under TOSCA. In order to find the Larmor radius corresponding to a particular  
1209 momentum, the matching procedure FIT can be used. In order to repeat the latter for  
1210 a series of different momenta, REBELOTE[IOPT=1] can be used.

1211 Explain why it is possible to push the ray-tracing beyond the 76 cm radial extent  
1212 of the field map.

1213 (c) Compute the orbit radius  $R$  and the revolution period  $T_{\text{rev}}$  as a function of  
1214 kinetic energy  $W$  or rigidity  $BR$ . Produce a graph, including for comparison the  
1215 theoretical dependence of  $T_{\text{rev}}$ .

1216 (d) Check the effect of the density of the mesh (the choice of  $\Delta R$  and  $\Delta\theta$  values,  
1217 *i.e.*, the number of nodes  $N_\theta \times N_R = (1 + \frac{180^\circ}{\Delta\theta}) \times (1 + \frac{80 \text{ cm}}{\Delta R})$ ), on the accuracy of the  
1218 trajectory and time-of-flight computation.

1219 (e) Consider a mesh with such  $\Delta R$ ,  $\Delta\theta$  density as to ensure reasonably good  
1220 convergence of the numerical resolution of the differential equation of motion [14,  
1221 Eq. 1.2.4].

1222 Check the effect of the integration step size on the accuracy of the trajectory  
1223 and time-of-flight computation, by considering a small  $\Delta s = 1$  cm and a large  
1224  $\Delta s = 20$  cm, at 200 keV and 5 MeV (proton).

1225 (f) Consider a periodic orbit, thus its radius  $R$  should remain unchanged after  
1226 stepwise integration of the motion over a turn. However, the size  $\Delta s$  of the numerical  
1227 integration step has an effect on the final value of the radius:

1228 for two different cases, 200 keV (a small orbit) and 5 MeV (a larger one), provide  
1229 the dependence of the relative error  $\delta R/R$  after one turn, on the integration step size  
1230  $\Delta s$  (consider a series of  $\Delta s$  values in a range  $\Delta s : 0.1 \text{ mm} \rightarrow 20 \text{ cm}$ ). Provide a  
1231 graph of the two  $\frac{\delta R}{R}(\Delta s)$  curves (200 keV and 5 MeV).

## 1232 4.2 Modeling a Cyclotron Dipole: Using an Analytical Field Model

1233 Solution: page 267

1234 This exercise is similar to exercise 4.1, yet using the analytical modeling DIPOLE,  
1235 instead of a field map. DIPOLE provides the  $Z$ -parallel median plane field  $\mathbf{B}(R, \theta, Z = 0) \equiv \mathbf{B}_Z(R, \theta, Z = 0)$  at the projected  $m(R, \theta, Z = 0)$  ion location (Fig. 4.18), while  
1236  $\mathbf{B}(R, \theta, Z)$  at particle location is obtained by extrapolation.

1237 (a) Simulate a  $180^\circ$  sector dipole; DIPOLE requires a reference radius [14,  
1238 Eqs. 6.3.19-21], noted  $R_0$  here; for the sake of consistency with other exercises, it is  
1239 suggested to take  $R_0 = 50$  cm. Take a constant axial field  $B_Z = 0.5$  T.  
1240

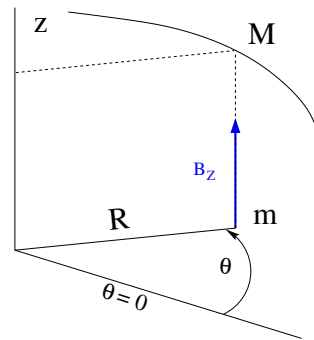


**Fig. 4.18** DIPOLE provides the value  $B_Z(m)$  of the median plane field at  $m$ , projection of particle position  $M(R, \theta, Z)$  in the median plane.  $\mathbf{B}(R, \theta, Z)$  is obtained by extrapolation

1241 Explain the various data that define the field simulation in DIPOLE: geometry,  
1242 role of  $R_0$ , field and field indices, fringe fields, integration step size, etc.

1243 Produce a graph of  $B_Z(R, \theta)$ .

1244 (b) Repeat question (b) of exercise 4.1.

1245 (c) Repeat question (c) of exercise 4.1.

1246 (d) As in question (e) of exercise 4.1, check the effect of the integration step size  
1247 on the accuracy of the trajectory and time-of-flight computation.

1248 Repeat question (f) of exercise 4.1.

1249 (e) From the two series of results (exercise 4.1 and the present one), comment on  
1250 various pros and cons of the two methods, field map versus analytical field model.

### 1251 4.3 Resonant Acceleration

1252 Solution: page 272

1253 Based on the earlier exercises, using indifferently a field map (TOSCA) or an  
1254 analytical model of the field (DIPOLE), introduce a sinusoidal voltage between the  
1255 two dees, with peak value 100 kV. Assume that ion motion does not depend on RF  
1256 phase: the boost through the gap is the same at all passes, use CAVITE[IOPT=3] [14,  
1257 cf. INDEX] for that. Note that using CAVITE requires prior PARTICUL in order to  
1258 specify ion species and data, necessary to compute the energy boost (Eq. 4.2).

1259 (a) Accelerate a proton with initial kinetic energy 20 keV, up to 5 MeV, take  
1260 harmonic  $h=1$ . Produce a graph of the accelerated trajectory in the laboratory frame.

1261 (b) Provide a graph of the proton momentum  $p$  and total energy  $E$  as a function  
1262 of its kinetic energy, both from this numerical experiment (ray-tracing data can be  
1263 stored using FAISTORE) and from theory, all on the same graph.

1264 (c) Provide a graph of the normalized velocity  $\beta = v/c$  as a function of kinetic  
1265 energy, both numerical and theoretical, and in the latter case both classical and  
1266 relativistic.

1267 (d) Provide a graph of the relative change in velocity  $\Delta\beta/\beta$  and orbit length  $\Delta C/C$   
1268 as a function of kinetic energy, both numerical and theoretical. From their evolution,  
1269 conclude that the time of flight increases with energy.

1270 (e) Repeat the previous questions, assuming a harmonic  $h=3$  RF frequency.

1271 **4.4 Spin Dance**

1272 Solution: page 275

1273 Cyclotron modeling in the present exercise can use Exercise 4.1 or Exercise 4.2  
1274 technique (*i.e.*, a field map or an analytical field model), indifferently.1275 (a) Add spin transport, using SPNTRK [14, *cf.* INDEX]. Produce a listing  
1276 (zgoubi.res) of a simulation, including spin outcomes.1277 Note: PARTICUL is necessary here, for the spin equation of motion (Eq. 4.27) to  
1278 be solved [14, Sect. 2]. SPNPRT can be used to have local spin coordinates listed in  
1279 zgoubi.res (at the manner that FAISCEAU lists local particle coordinates).1280 (b) Consider proton case, take initial spin longitudinal, compute the spin preces-  
1281 sion over one revolution, as a function of energy over a range 12 keV→5 MeV. Give  
1282 a graphical comparison with theory.1283 FAISTORE can be used to store local particle data, which include spin coordi-  
1284 nates, in a zgoubi.fai style output file. IL=2 [14, *cf.* INDEX] (under DIPOLE or  
1285 TOSCA, whichever modeling is used) can be used to obtain a print out of particle  
1286 and spin motion data to zgoubi.plt during stepwise integration.1287 (c) Inject a proton with longitudinal initial spin  $S_i$ . Give a graphic of the lon-  
1288 gitudinal spin component value as a function of azimuthal angle, over a few turns  
1289 around the ring. Deduce the spin tune from this computation. Repeat for a couple of  
1290 different energies.1291 Place both FAISCEAU and SPNPRT commands right after the first dipole sector,  
1292 and use them to check the spin rotation and its relationship to particle rotation, right  
1293 after the first passage through that first sector.1294 (d) Spin dance: the input data file optical sequence here is assumed to model a  
1295 full turn. Inject an initial spin at an angle from the horizontal plane (this is in order  
1296 to have a non-zero vertical component), produce a 3-D animation of the spin dance  
1297 around the ring, over a few turns.1298 (e) Repeat questions (b-d) for two additional ions: deuteron (much slower spin  
1299 precession),  ${}^3\text{He}^{2+}$  (much faster spin precession).1300 **4.5 Synchronized Spin Torque**

1301 Solution: page 281

1302 A synchronized spin kick is superimposed on orbital motion. An input data file for  
1303 a complete cyclotron is considered as in question 4.4 (d), for instance six 60 degree  
1304 DIPOLES, or two 180 degree DIPOLES.1305 Insert a local spin rotation of a few degrees around the longitudinal axis, at the  
1306 end of the optical sequence (*i.e.*, after one orbit around the cyclotron). SPINR  
1307 can be used for that, to avoid any orbital effect. Track 4 particles on their closed orbit,  
1308 with respective energies 0.2, 108.412, 118.878 and 160.746 MeV.1309 Produce a graph of the motion of the vertical spin component  $S_y$  along the circular  
1310 orbit.

1311 Produce a graph of the spin vector motion on a sphere.

1312 **4.6 Weak Focusing**

1313 Solution: page 285

1314 (a) Consider a  $60^\circ$  sector as in earlier exercises (building a field map and using  
 1315 TOSCA as in exercise 4.1, or using DIPOLE as in exercise 4.2), construct the sector  
 1316 accounting for a non-zero radial index  $k$  in order to introduce axial focusing, say  
 1317  $k = -0.03$ , assume a reference radius  $R_0$  for a reference energy of 200 keV ( $R_0$  and  
 1318  $B_0$  are required in order to define the index  $k$ , Eq. 4.10). Ray-trace that 200 keV  
 1319 reference orbit, plot it in the lab frame: make sure it comes out as expected, namely,  
 1320 constant radius, final and initial angles zero.

1321 (b) Find and plot the radius dependence of orbit rigidity,  $BR(R)$ , from ray-tracing  
 1322 over a  $BR$  range covering 20 keV to 5 MeV; superpose the theoretical curve. REBE-  
 1323 LOTE can be used to perform the scan.

1324 (c) Produce a graph of the paraxial axial motion of a 1 MeV proton, over a few  
 1325 turns (use IL=2 under TOSCA, or DIPOLE, to have step by step particle and field  
 1326 data logged in zgoubi.plt). Check the effect of the focusing strength by comparing  
 1327 the trajectories for a few different index values, including close to -1 and close to 0.

1328 (d) Produce a graph of the magnetic field experienced by the ion along these  
 1329 trajectories.

#### 1330 4.7 Loss of Isochronism

1331 Solution: page 294

1332 Compare on a common graphic the revolution period  $T_{\text{rev}}(R)$  for a field index  
 1333 value  $k \approx -0.95, -0.5, -0.03, 0^-$ . The scan method of exercise 4.6, based on  
 1334 REBELOTE, can be referred to.

#### 1335 4.8 Ion Trajectories

1336 Solution: page 296

1337 In this exercise individual ion trajectories are computed. DIPOLE or TOSCA  
 1338 magnetic field modeling can be used, indifferently. No acceleration here, ions cycle  
 1339 around the cyclotron at constant energy.

1340 (a) Produce a graph of the horizontal and vertical trajectory components  $x(s)$   
 1341 and  $y(s)$  of an ion with rigidity close to  $BR(R_0)$  ( $R_0$  is the reference radius in the  
 1342 definition of the index  $k$ ), over a few turns around the cyclotron. From the number of  
 1343 turns, give an estimate of the wave numbers. Check the agreement with the expected  
 1344  $\nu_R(k), \nu_y(k)$  values (Eq. 4.15).

1345 (b) Consider now protons at 1 MeV and 5 MeV, far from the reference energy  
 1346  $E(R_0)$ ; the wave numbers change with energy: consistency with theory can be  
 1347 checked. Find their theoretical values, compare with numerical outcomes.

1348 (c) Consider proton, 200 keV energy, plot as a function of  $s$  the difference between  
 1349  $x(s)$  from raytracing and its values from Eq. 4.13. Same for  $y(s)$  compared to Eq. 4.14.  
 1350 IL=2 can be used to store in zgoubi.plt the step-by-step particle coordinates across  
 1351 DIPOLE.

1352 (d) Perform a scan of the wave numbers over 200 keV–5 MeV energy interval,  
 1353 computed using MATRIX, and using REBELOTE to repeat MATRIX for a series  
 1354 of energy values.

1355 **4.9 RF Phase at the Accelerating Gap**

1356 Solution: page 302

1357 Consider the cyclotron model of exercise 4.6: field index  $k = -0.03$  defined at  
1358  $R_0 = 50$  cm, field  $B_0 = 5$  kG on that radius. two dees, double accelerating gap.

1359 Accelerate a proton from 1 to 5 MeV: get the turn-by-turn phase-shift at the gaps;  
1360 use CAVITE[IOPT=7] to simulate the acceleration. Compare the half-turn  $\Delta\phi$  so  
1361 obtained with the theoretical expectation (Eq. 4.22). Produce similar graphs  $B(R)$   
1362 and  $\Delta W(\phi)$  to Fig. 4.13.

1363 Accelerate over more turns, observe the particle decelerating.

1364 **4.10 The Cyclotron Equation**

1365 Solution: page 304

1366 The cyclotron model of exercise 4.3 is considered: two dees, double accelerating  
1367 gap, uniform field  $B = 0.5$  T, no gradient.

1368 (a) Set up an input data file for the simulation of a proton acceleration from  
1369 0.2 to 20 MeV. In particular, assume that  $\cos(\phi)$  reaches its maximum value at  
1370  $W_m = 10$  MeV; find the RF voltage frequency from  $d(\cos \phi)/dW = 0$  at  $W_m$ .

1371 (b) Give a graph of the energy-phase relationship (Eq. 4.23), for  $\phi_i = \frac{3\pi}{4}, \frac{\pi}{2}, \frac{\pi}{4}$ ,  
1372 from both simulation and theory.

1373 **4.11 Cyclotron Extraction**

1374 Solution: page 306

1375 (a) Acceleration of a proton in a uniform field  $B=0.5$  T is first considered (field  
1376 hypotheses as in exercise 4.3). RF phase is ignored: CAVITE[IOPT=3] can be used  
1377 for acceleration. Take a 100 kV gap voltage.

1378 Compute the distance  $\Delta R$  between turns, as a function of turn number and of  
1379 energy, over the range  $E : 0.02 \rightarrow 5$  MeV. Compare graphically with theoretical  
1380 expectation.

1381 (b) Assume a beam with Gaussian momentum distribution and *rms* momentum  
1382 spread  $\delta p/p = 10^{-3}$ . An extraction septum is placed half-way between two successive  
1383 turns, provide a graph of the percentage of beam loss at extraction, as a function of  
1384 extraction turn number - COLLIMA can be used for that simulation and for particle  
1385 counts, it also allows for possible septum thickness.

1386 (c) Repeat (a) and (b) considering a field with index: take for instance  $B_0 = 0.5$  T  
1387 and  $k = -0.03$  at  $R_0 = R(0.2 \text{ MeV}) = 12.924888$  cm.

1388 (d) Investigate the effect of injection conditions ( $Y_i, T_i$ ) on the modulation of the  
1389 distance between turns.

1390 Show numerically that, with slow acceleration, the oscillation is minimized for  
1391 an initial  $|T_i| = \left| \frac{x_0 v_R}{R} \right|$  (after Ref. [9, p. 133]).

1392 **4.12 Acceleration and Extraction of a 6-D Polarized Bunch**

1393 Solution: page 311

1394 The cyclotron simulation hypotheses of exercise 4.10-a are considered.

1395 Add a short “high energy” extraction line, say 1 meter, following REBELOTE in  
 1396 the optical sequence, ending up with a “Beam\_Dump” MARKER for instance.

1397 (a) Create a 1,000 ion bunch with the following initial parameters:

1398 - random Gaussian transverse phase space densities, centered on the closed orbit,  
 1399 truncated at 3 sigma, normalized *rms* emittances  $\varepsilon_Y = \varepsilon_Z = 1 \pi \mu\text{m}$ , both emittances  
 1400 matched to the 0.2 MeV orbit optics,

1401 - uniform bunch momentum density  $0.2 \times (1 - 10^{-3}) \leq p \leq 0.2 \times (1 + 10^{-3}) \text{ MeV}$ ,  
 1402 matched to the dispersion, namely (Eq. 4.18),  $\Delta x = D \frac{\Delta p}{p}$ ,

1403 - random uniform longitudinal distribution  $-0.5 \leq s \leq 0.5 \text{ mm}$ ,

1404 Note: two ways to create this object are, (i) using MCOBJET[KOBJ=3] which  
 1405 generates a random distribution, or (ii) using OBJET[KOBJ=3] to read an external  
 1406 particle coordinate file.

1407 Add spin tracking request (SPNTRK), all initial spins normal to the bend plane.

1408 Produce a graph of the three initial 2-D phase spaces: (Y,T), (Z,P), ( $\delta l, \delta p/p$ ),  
 1409 matched to the 200 keV periodic optics. Provide Y, Z, dp/p,  $\delta l$  and  $S_Z$  histograms,  
 1410 check the distribution parameters.

1411 (b) Accelerate this polarized bunch to 20 MeV, using the following RF conditions:

1412 - 200 kV peak voltage,

1413 - RF harmonic 1,

1414 - initial RF phase  $\phi_i = \pi/4$ .

1415 Produce a graph of the three phase spaces as observed downstream of the extrac-  
 1416 tion line. Provide the Y, Z, dp/p,  $\delta l$  and  $S_Z$  histograms. Compare the distribution  
 1417 parameters with the initial values.

1418 What causes the spins to spread away from vertical?



1419 **References**

- 1420 1. Jones, L., Mills, F., Sessler, A., et al.: Innovation Was Not Enough. World Scientific (2010)
- 1421 2. Lawrence, E.O., Livingston, M.S. Phys. Rev. 37, 1707 (1931), 1707; Phys. Rev. 38, 136,
- 1422 (1931); Phys. Rev. 40, 19 (1932)
- 1423 3. Credit: Lawrence Berkeley National Laboratory. ©The Regents of the University of California,
- 1424 Lawrence Berkeley National Laboratory
- 1425 4. Lawrence, E.O. and Livingston, M.S.: The Production of High Speed Light Ions Without the
- 1426 Use of High Voltages. Phys. Rev. 40, 19-35 (1932)
- 1427 5. Livingston, M.S., McMillan, E.M.: History of the cyclotron. Physics Today, 12(10) (1959).
- 1428 <https://escholarship.org/uc/item/29c6p35w>
- 1429 6. Bethe, H. E., Rose, M. E.: Maximum energy obtainable from cyclotron. Phys. Rev. 52 (1937)
- 1430 1254
- 1431 7. Cole, F.T.: O Camelot ! A memoir of the MURA years (April 1, 1994).
- 1432 <https://accelconf.web.cern.ch/c01/cyc2001/extra/Cole.pdf>
- 1433 8. 4.a Thomas, L.H.: The Paths of Ions in the Cyclotron. Phys. Rev. 54, 580, (1938)
- 1434 4.b Craddock, M.K.: AG focusing in the Thomas cyclotron of 1938. Proceedings of PAC09,
- 1435 Vancouver, BC, Canada, FR5REP1
- 1436 9. Stambach, T.: Introduction to Cyclotrons. CERN accelerator school, cyclotrons, linacs and
- 1437 their applications. IBM International Education Centre, La Hulpe, Belgium, 28 April-5 May
- 1438 1994
- 1439 10. Credit: CERN Accelerator School. Stambach, T.: Introduction to Cyclotrons. CERN Yellow
- 1440 Report 96-02 (1996), Figure 8, page 15, unchanged. Copyright/License CERN CC-BY-3.0 -
- 1441 <https://creativecommons.org/licenses/by/3.0>
- 1442 11. Baron, E., et al.: The GANIL Injector. Proceedings of the 7th International Conference on
- 1443 Cyclotrons and their Applications, Zürich, Switzerland (1975).
- 1444 <http://accelconf.web.cern.ch/c75/papers/b-05.pdf>
- 1445 12. Le Duff, J.: Longitudinal beam dynamics in circular accelerators. CERN Accelerator School,
- 1446 Jyväskylä, Finland, 7-18 September 1992
- 1447 13. Méot, F.: Spin Dynamics. USPAS Summer 2021 Spin Class Lectures. Springer (2023)
- 1448 14. Méot, F.: Zgoubi Users' Guide.
- 1449 <https://www.osti.gov/biblio/1062013-zgoubi-users-guide> Sourceforge latest version:
- 1450 <https://sourceforge.net/p/zgoubi/code/HEAD/tree/trunk/guide/Zgoubi.pdf>